Supplementary material for:

First-principles study of defects and doping limits in CaO

Zhenkun Yuan and Geoffroy Hautier*

Thayer School of Engineering, Dartmouth College, Hanover, New Hampshire 03755, USA

Email: geoffroy.hautier@dartmouth.edu

Computational details

Defect formation energies were calculated using the standard formalism as described in Refs. 1 and 2. As an example, the formation energy of V_O^q, i.e., the oxygen vacancy (V_O) in the charge state q, is given by

$$E_f\left(V_O^q\right) = E_{tot}\left(V_O^q\right) - E_{tot}(\text{bulk}) + \mu_O + qE_F + \Delta^q,$$

where $E_{tot}\left(V_O^q\right)$ and $E_{tot}(\text{bulk})$ are the total energies of the supercell containing the V_O^q and the bulk (i.e., defect-free) supercell, respectively. The last term, Δ^q, is a finite-supercell-size correction to $E_{tot}\left(V_O^q\right)$ accounting for the spurious electrostatic interaction between the charged defect and its periodic images,[3, 4] and was calculated using the experimental static dielectric constant ($\varepsilon_0 = 11.95$).[5] The formation of V_O^q involves exchanging an oxygen atom and $|q|$ electrons with the atomic and electron reservoirs, whose chemical potentials are μ_O and E_F, respectively. The electron chemical potential (E_F), i.e., the Fermi level, is referenced to the valence-band maximum (VBM) and ranges over the CaO band gap. The chemical potentials of Ca (μ_{Ca}) and O (μ_O) are referenced to the total energies per atom of their respective elemental phase (fcc Ca metal and O$_2$ molecule, respectively). The elemental chemical potentials are treated as variables so as to reflect experimental growth conditions for CaO.

In thermodynamic equilibrium, the elemental chemical-potentials are bound by $\mu_{Ca}, \mu_O \leq 0$ and $\mu_{Ca} + \mu_O = \Delta H_f(\text{CaO})$, which prevent the formation of Ca bulk metal and O$_2$ molecules, and ensure thermodynamic stability of CaO. The $\Delta H_f(\text{CaO})$ is the formation enthalpy of CaO and calculated to be -6.23 eV, close to the experimental value of -6.58 eV.[6] As a result, μ_O can vary from -6.23 eV (the O-poor limit) to 0 eV (the O-rich limit). In calculating the defect formation energies, $\mu_O = -6.23$ and 0 eV, are chosen to represent O-poor and O-rich growth conditions for CaO, respectively. To relate μ_O to the experimental conditions in terms of temperature and oxygen partial pressure, we rely on the ideal-gas model:[7]

$$\mu_O = \frac{1}{2}\left[-TS_{O_2} + RT\ln p_{O_2}\right],$$

where S_{O_2} is the experimentally measured standard entropy of O$_2$ gas,[8] R the ideal-gas constant, p_{O_2} the O$_2$ partial pressure, and T the temperature. μ_O is referenced to $\frac{1}{2}E_{tot}(O_2)$, i.e., one half of the total energy of the O$_2$ molecule at 0 K. We find that experimentally, to obtain $\mu_O = -6.23$ eV, a temperature as high as 3000 K and an oxygen partial pressure as low as 10^{-10} bar are needed, for example. Such a high temperature would be challenging to realize.[9]

The formation energy of the hydrogen-related defects depends on the hydrogen chemical potential (μ_H). Assuming that hydrogen inside CaO is in equilibrium with H$_2$ molecules in the growth or annealing environment, μ_H can be defined through the ideal-gas model:

$$\mu_{\mathrm{H}} = \frac{1}{2}\left[-TS_{\mathrm{H}_2} + RT\ln p_{\mathrm{H}_2}\right],$$

where S_{H_2} is the experimentally measured standard entropy of H_2 gas,[8] R the ideal-gas constant, and p_{H_2} the H_2 partial pressure. μ_{H} is referenced to $\frac{1}{2}E_{\mathrm{tot}}(\mathrm{H}_2)$, i.e., one half of the total energy of the H_2 molecule at 0 K. We considered temperature of 1000 K, and varied p_{H_2} from 10^{-10} to 1 bar; correspondingly, this leads to μ_{H} values in the range -1.67 to -0.68 eV. There exist upper bounds of μ_{H}, arising from solubility-limiting phases. This depends on μ_{O}. For $\mu_{\mathrm{O}} = -6.23$ eV (the O-poor limit), the maximum allowed value of μ_{H} is 0 eV and limited by formation of H_2 molecules; for $\mu_{\mathrm{O}} = 0$ eV (the O-rich limit), the maximum allowed value of μ_{H} is -1.97 eV and limited by formation of $Ca(OH)_2$. The latter implies that under O-rich conditions, exposure to H_2 gas should be avoided in order not to cause hydrogenation of CaO forming $Ca(OH)_2$.[10]

The binding energies of $[\mathrm{H} + V_{\mathrm{Ca}}]^-$ and $[2\mathrm{H} + V_{\mathrm{Ca}}]^0$ were obtained as the difference between the formation energy of the complexes and the sum of the formation energies of isolated V_{Ca}^{2-} and H_i^+. They are independent of elemental chemical potentials due to a cancelation of terms.

In thermodynamic equilibrium, the defect concentration is given by $c[\mathrm{X}^q] = N_{\mathrm{sites}}\exp\left(-\frac{E_{\mathrm{f}}(\mathrm{X}^q)}{k_B T}\right)$, where N_{sites} is the number of sites (per unit volume) at which the defect can form.[11] This equation shows that in equilibrium, a defect with low formation energy has high concentration. Using the calculated defect formation energies, the Fermi level can be determined by the charge-neutrality condition, accounting for all charged defects and free carriers in the bands.[12-15] We obtained the defect concentrations, Fermi-level position, and carrier densities using the py-sc-fermi code.[14]

The PyCDT code was used to generate defect initial structures and postprocess the defect calculations.[16] To correctly identify the lowest-energy configuration of the interstitial defects $(\mathrm{Ca}_i, \mathrm{O}_i, \text{and } \mathrm{H}_i)$, a number of trial interstitial sites were examined, and this was done for different charge states. Besides, the ShakeNBreak code[17, 18] was also used to generate initial structures for the most important charged defects, V_{Ca}^{2-}, V_{O}^+, and V_{O}^{2+}.

Local geometry of the intrinsic defects in CaO

Here we show the local geometry of the intrinsic defects in their important charge states.
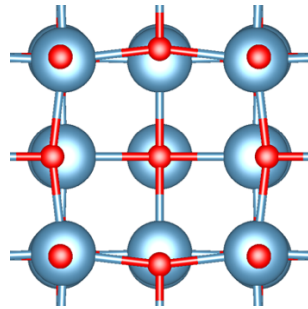
FIG. S1. Calcium vacancy in the 2− charge state, i.e., V_{Ca}^{2-}. The red and cyan balls denote oxygen and calcium atoms, respectively (same in the following figures). The VESTA software was used for the plot.[19]
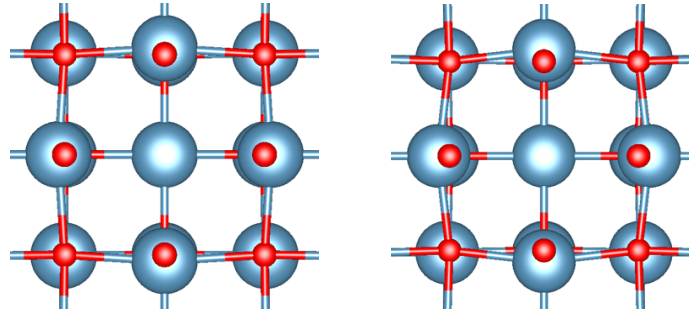
FIG. S2. Oxygen vacancy in the 1+ (left) and 2+ (right) charge states, i.e., V_O^+ and V_O^{2+}, respectively.
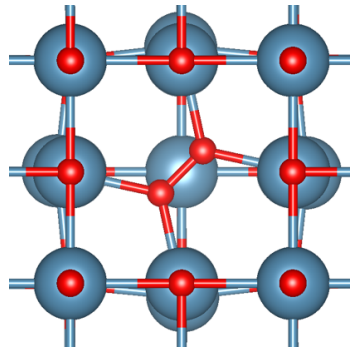
FIG. S3. Oxygen interstitial in the neutral charge state, i.e., O_i^+, which adopts a split-interstitial configuration.
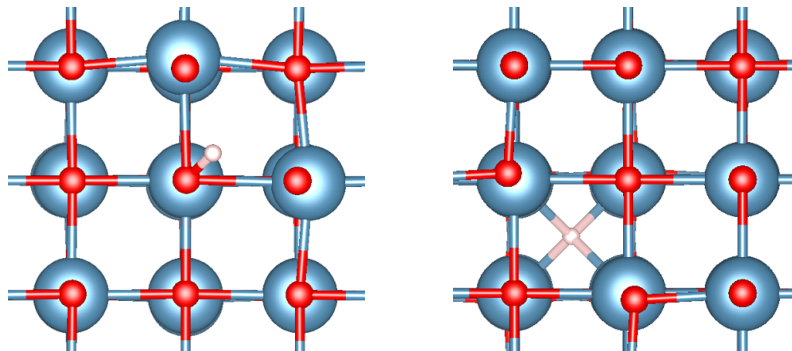
FIG. S4. Hydrogen interstitial in the 1+ (left) and 1− (right) charge states, i.e., H_i^+ and H_i^-, respectively. The light pink ball denotes the hydrogen atom.
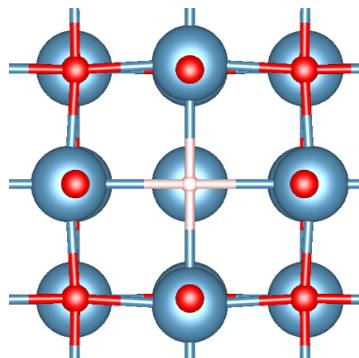
FIG. S5. Hydrogen substitution on the oxygen site in the 1+ charge state, i.e., H_O^+.

Defect charge-state transition levels, single-particle defect states, and defect concentrations

Table S1. Defect charge-state transition levels (in unit of eV) referenced to the VBM of CaO. Included only the transition levels in the CaO band gap.

Defect species	$\epsilon(q/q')$
V_{Ca}	(2+/+) 1.33, (+/0) 1.62, (0/−) 1.81, (−/2−) 2.11
V_O	(2+/+) 3.20, (+/0) 5.06
Ca_O	(4+/3+) 0.53, (3+/2+) 3.87, (2+/+) 6.07
O_{Ca}	(+/0) 0.89, (0/2−) 2.37, (2−/4−) 4.94
Ca_i	(2+/+) 6.43, (+/0) 6.92
O_i	(2+/+) 0.85, (+/0) 1.38, (0/2−) 4.79
H_i	(+/−) 5.0
H_O	(+/0) 7.085
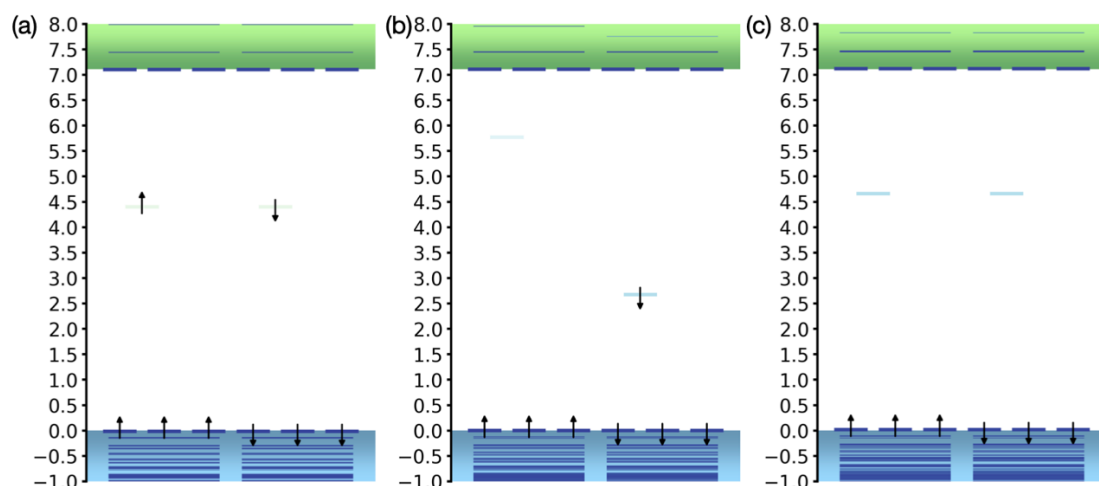
FIG. S6. Single-particle defect states for V_O in the (a) 0, (b) 1+, and (c) +2 charge states in the band gap of CaO.
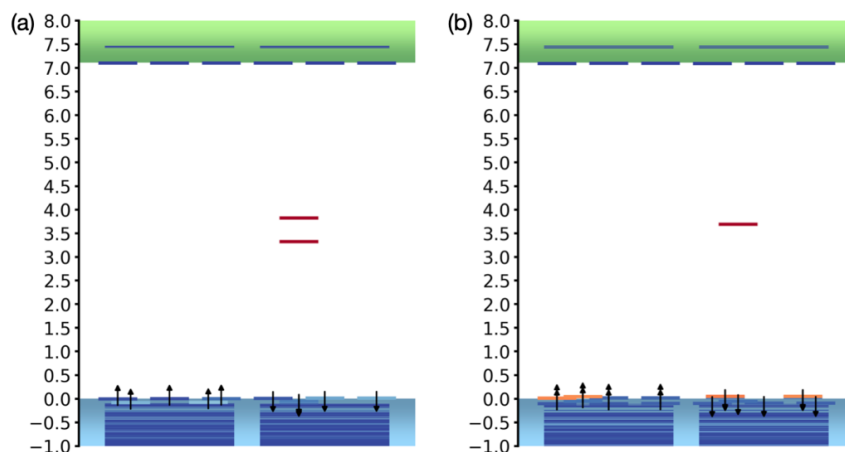
FIG. S7. Single-particle defect states for V_{Ca} in the (a) 0 and (b) 1− charge states in the band gap of CaO.
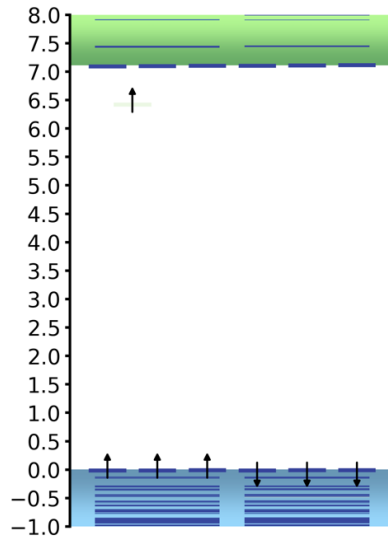
FIG. S8. Single-particle defect states for H_O in the neutral charge state in the band gap of CaO.

Table S2. Defect concentrations in O-poor CaO grown at 1000 K and rapidly quenched to 300 K. The results correspond to the defect formation energies in Fig. 1(a) in the main text. Other defect species have negligible concentrations. Without the quenching, the V_O^+ concentration would be 1.20×10^{14} cm^{-3}.

Defect species	Concentration (cm^{-3})
V_{Ca}^{2-}	5.59×10^{12}
V_O^0	5.06×10^{17}
V_O^+	1.12×10^{13}

References

1. S. B. Zhang, S.-H. Wei, A. Zunger and H. Katayama-Yoshida, Phys. Rev. B **57**, 9642 (1998).
2. C. Freysoldt, B. Grabowski, T. Hickel, J. Neugebauer, G. Kresse, A. Janotti and C. G. Van de Walle, Rev. Mod. Phys. **86**, 253 (2014).
3. C. Freysoldt, J. Neugebauer and C. G. Van de Walle, Phys. Rev. Lett. **102**, 016402 (2009).
4. Y. Kumagai and F. Oba, Phys. Rev. B **89**, 195205 (2014).
5. M. A. Subramanian, R. D. Shannon, B. H. T. Chai, M. M. Abraham and M. C. Wintersgill, Phys. Chem. Miner. **16**, 741 (1989).
6. W. Haynes, D. Lide and T. Bruno, *CRC handbook of chemistry and physics*, 95th ed. (CRC Press, 2016).
7. K. Reuter and M. Scheffler, Phys. Rev. B **65**, 035406 (2001).
8. M. W. C. Jr, *NIST-JANAF Thermochemical Tables*, Fourth ed. (1998).
9. K.T. Jacob and S. Srikanth, High Temperature Materials and Processes **9**, 77 (1990).
10. N. A. Surplice, Br. J. Appl. Phys. **17**, 175 (1966).
11. C. G. Van de Walle and J. Neugebauer, J. Appl. Phys. **95**, 3851 (2004).
12. Y. Kumagai, M. Choi, Y. Nose and F. Oba, Phys. Rev. B **90**, 125202 (2014).
13. J.-H. Yang, J.-S. Park, J. Kang, W. Metzger, T. Barnes and S.-H. Wei, Phys. Rev. B **90**, 245202 (2014).
14. A. G. Squires, D. O. Scanlon and B. J. Morgan, J. Open Source Softw. **8**, 4962 (2023).
15. J. Buckeridge, Comput. Phys. Commun. **244**, 329 (2019).
16. D. Broberg, B. Medasani, N. E. R. Zimmermann, G. Yu, A. Canning, M. Haranczyk, M. Asta and G. Hautier, Comput. Phys. Commun. **226**, 165 (2018).
17. I. Mosquera-Lois, S. R. Kavanagh, A. Walsh and D. O. Scanlon, J. Open Source Softw. **7**, 4817 (2022).
18. S. R. Kavanagh, A. G. Squires, A. Nicolson, I. Mosquera-Lois, A. M. Ganose, B. Zhu, K. Brlec, A. Walsh and D. O. Scanlon, J. Open Source Softw. **9**, 6433 (2024).
19. K. Momma and F. Izumi, J. Appl. Crystallogr. **44**, 1272 (2011).